



Astrophysical Properties of 600 Bona Fide Single Stars in the Hyades Open Cluster

Wolfgang Brandner¹ , Per Calissendorff² , and Taisiya Kopytova^{1,3} ¹Max-Planck-Institut für Astronomie Königstuhl 17 D-69117 Heidelberg, Germany; brandner@mpia.de²Department of Astronomy University of Michigan Ann Arbor, MI 4810, USA³Ural Federal University Yekaterinburg 620002, Russia

Received 2022 December 22; revised 2023 January 9; accepted 2023 January 9; published 2023 February 15

Abstract

The determination of the astrophysical properties of stars remains challenging and frequently relies on the application of stellar models. Stellar sequences in nearby open clusters provide some of the best means to test and calibrate stellar evolutionary models and isochrones and to use these models to assign astrophysical properties consistently to a large sample of stars. We aim at updating the single-star sequence of the members of the Hyades cluster, identifying the best-fitting isochrones, and determining the astrophysical properties of the stars. The Gaia Catalog of Nearby Stars provides a comprehensive sample of high-probability members of the Hyades cluster. We apply a multistep method to flag photometric outliers and to identify bona fide single stars and likely binary and multiple systems. The single stars define a tight sequence, which in the mass range $0.12\text{--}2.2 M_{\odot}$ is well fitted by PARSEC isochrones for a supersolar metallicity of $[M/H] = +0.18 \pm 0.03$ and an age of 775 ± 25 Myr. The isochrones enable us to assign mass, effective temperature, luminosity, and surface gravity to each of the 600 bona fide single main-sequence stars. The observed sequence validates the PARSEC isochrones. The derived stellar properties can serve as benchmarks for atmospheric and evolutionary models and for all-sky catalogs of stellar astrophysical properties. The stellar properties are also relevant for studies of exoplanet properties among Hyades exoplanet hosts.

Unified Astronomy Thesaurus concepts: Open star clusters (1160); Stellar evolution (1599); Stellar dynamics (1596); Stellar colors (1590); Stellar effective temperatures (1597); Stellar luminosities (1609); Stellar masses (1614); Young star clusters (1833); Stellar abundances (1577); Stellar properties (1624); Stellar ages (1581); Stellar types (1634)

Supporting material: machine-readable table

1. Introduction

Studies of protocluster environments and Galactic starburst clusters at ages well below 10 Myr suggest that clustered star formation occurs quasi-instantaneously, with a maximum age spread among cluster members of the order of 0.1–0.4 Myr (Kudryavtseva et al. 2012; Parmentier et al. 2014; Williams et al. 2022). Galactic open clusters with typical ages of a few to several 100 Myr also exhibit small spreads in age and metallicity among their members, suggesting close-to-coeval formation out of the homogeneously mixed material of the parental giant molecular cloud (Bovy 2016; Jeffries 2017; Magrini et al. 2017; Krumholz & McKee 2020).

Star clusters are thus suited particularly well for studying stellar astrophysical properties as a function of stellar mass or its proxies stellar effective temperature and luminosity. Due to its proximity and richness in stellar members, the nearby Hyades open cluster is frequently used for testing and calibrating stellar evolutionary models (Castellani et al. 2001; Kopytova et al. 2016; Jeffery et al. 2022).

Based on Gaia Early Data Release 3 (EDR3) astrometry and radial velocities, Gaia Collaboration et al. (2021) identify more than 3000 potential members of the Hyades cluster within 100 pc of the Sun. After application of a local density filter, they reduce this to a sample of 920 candidate members. Brandner et al. (2023) use this sample as a basis for benchmarking MESA evolutionary

models (Choi et al. 2016; Dotter 2016) and find a significant discrepancy between the observational sequence and theoretical isochrones in the stellar mass range $0.25\text{--}0.85 M_{\odot}$.

A possible fix to resolve this discrepancy is a modification of the temperature–Rosseland mean optical depth relation ($T\text{--}\tau$) in the stellar models, as introduced by Chen et al. (2014) for the PAdova and TRieste Stellar Evolution Code (PARSEC; Girardi et al. 2002; Marigo et al. 2008; Bressan et al. 2012).

In the present paper, we test PARSEC isochrones against the cleaned-up single-star sequence of the Hyades open cluster and use the family of best-fitting isochrones to assign astrophysical properties to 600 candidate members of the Hyades. The structure of the paper is as follows: in Section 2 we describe the processing of the Gaia data and the identification of the single stars. In Section 3 we identify the best-fitting PARSEC isochrones and determine the stellar properties. In Section 4 we close with a discussion and outlook.

2. The Single-star Sequence: Cleaning the Gaia Data Set

While in general of exquisite and unprecedented quality, Gaia DR3 does include some problematic data. This in particular concerns bright sources saturating too many pixels on the Gaia detectors and faint sources that can be subject to photometric blends in particular in the spectrally dispersed blue (BP) and red (RP) passbands. The Gaia Catalog of Nearby Stars (GCNS) also includes faint red stars with significant detections in the G and RP bands and with BP magnitudes at or below the formal Gaia detection limit (Gaia Collaboration et al. 2021).

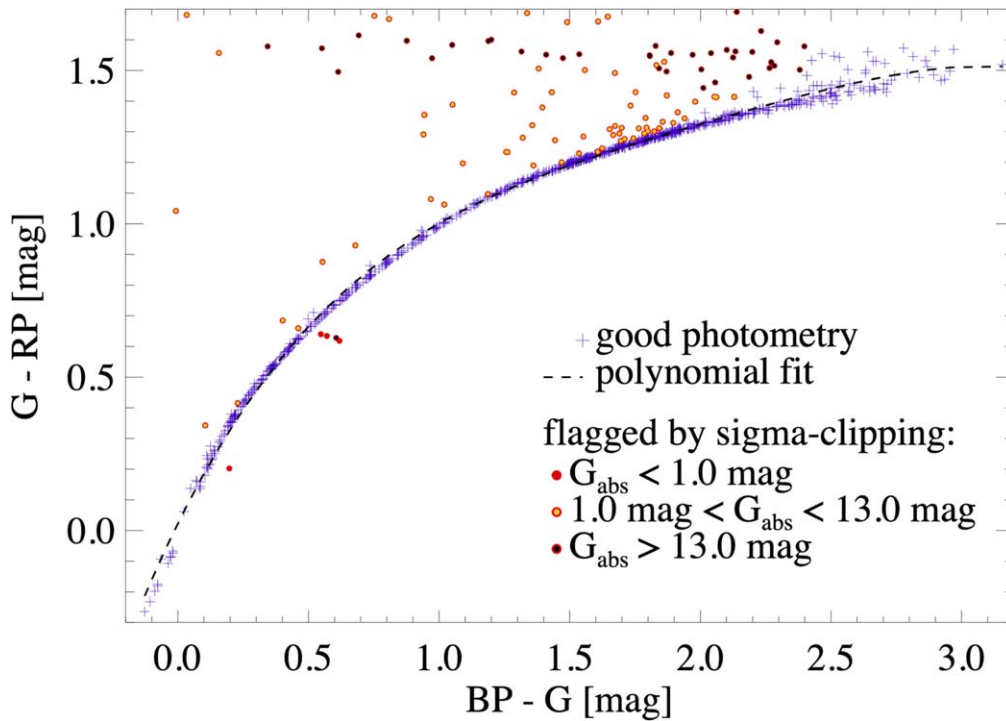


Figure 1. Color-color-magnitude diagram of the Hyades open cluster based on Gaia DR3 photometry. Bluish-purple cross symbols mark sources with valid photometry in all three Gaia photometric bands. The circles mark stars with potentially unreliable photometry in at least one of the photometric bands as identified by sigma clipping.

In Brandner et al. (2023) we defined a multistep process to classify the 920 GCNS candidate members of the Hyades open cluster into four groups: bona fide single stars, probable binary and multiple systems, white dwarfs, and sources with problematic photometry in at least one of the Gaia photometric bands. In order to flag sources with potentially unreliable photometry, we iteratively fit a fourth-order polynomial to the Gaia DR3⁴ data in G - RP versus BP - G color-color space and then apply sigma clipping at the 3σ level (Figure 1), resulting in 783 sources with reliable photometry. The stars flagged with potentially unreliable photometry fall into three classes: i) four giant stars (δ Tau, ϵ Tau, γ Tau, and Θ^2 Tau; red filled circles) in the Hyades with $G_{\text{abs}} < 1$ mag, which are brighter than the nominal saturation limit of Gaia (E)DR3 (Riello et al. 2021, Appendix C.1); ii) 38 stars with $G_{\text{abs}} > 13$ mag (yellow circles with red outline). These stars have $\langle G \rangle_{\text{median}} \approx 19.5$ mag and an apparent BP brightness below the nominal Gaia epoch detection threshold of $BP = 20.3$ mag, which results in an overestimate of the mean flux (Riello et al. 2021, Section 8.1). In the two-color diagram of Figure 1, these stars occupy a band around G - $RP \approx 1.5$ – 1.6 mag, the only exception being Gaia EDR3 1988661087451017856, which has a photogeometric distance of ≈ 96 pc (Bailer-Jones et al. 2021) and is classified as a candidate white dwarf by Gentile Fusillo et al. (2021); iii) 67 stars with $1 \text{ mag} < G_{\text{abs}} < 13$ mag, which have $\langle G \rangle_{\text{median}} \approx 13.9$ mag (black circles with red outline). In the two-color diagram, these stars are all located to the left (bluer BP - G color) and above (redder G - RP color) of the typical sequence defined by the photospheres of Hyades members. We were not

able to assign any plausible astrophysical reason for their peculiar Gaia colors.

Next we use the re-normalized unit weight error (RUWE; see GAIA-Collaboration 2020; Lindegren et al. 2021) to classify stars with $\text{RUWE} < 1.4$ as bona fide single stars. The sensitivity of the astrometric selection varies with projected separation, orbital period, and mass ratio of the binaries. Very close binaries, for example, are in general not identified by the RUWE selection. In a color-absolute-magnitude diagram, though, binaries composed of two main-sequence stars stand out as being brighter sources located above and potentially redward of the single-star main sequence (see, e.g., Elson et al. 1998). Similarly, binaries composed of a main-sequence star and a white dwarf (such as HZ 9; see Section 2) would be located blueward (and below) of the single-star main sequence. In order to reject these sources from the sequence of bona fide single stars, we iteratively fitted an eighth order polynomial and applied sigma clipping at the 3σ level in a color-absolute magnitude diagram to all sources classified to have good photometry and with $\text{RUWE} \leq 1.4$. After the convergence of the iterative process, the majority of the sources on the binary sequence are flagged as likely binaries.

Golovin et al. (2023) discuss that the distinction between likely binary and multiple systems and bona fide single stars at $\text{RUWE} = 1.4$ irrespective of G -band magnitude or BP - RP color might introduce a bias in terms of sample completeness. For the Hyades sample, though, the effect is small. Using, for example, 1.2 times the sliding window median value of RUWE as a function of G as the dividing line would add three stars with $G < 5$ mag and eight stars with $10.5 < G < 14.5$ mag to—and remove 10 stars with $G > 15$ mag from—our sample of ≈ 600 bona fide single stars (Figure 2).

For the transformation to absolute G magnitudes, we use the photogeometric distance estimates from Bailer-Jones et al. (2021). In Figure 3 we show the color-absolute-magnitude diagram of the

⁴ In Brandner et al. (2023) we used Gaia EDR3 G magnitudes, which had not been corrected for the processing error described in Section 8.3 of Riello et al. (2021). This error, which amounts to up to 0.0025 mag, affected 100 of the 920 GCNS candidate members of the Hyades.

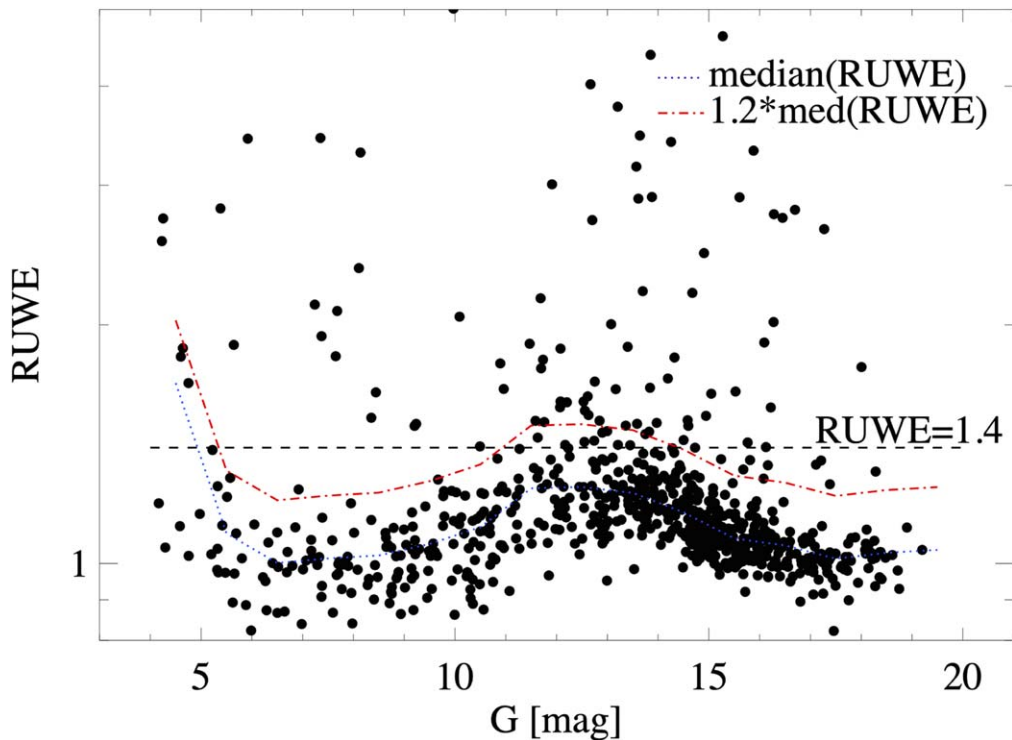


Figure 2. RUWE as a function of G . The dashed line marks the canonical border line between likely binary and multiple systems with $\text{RUWE} > 1.4$ and bona fide single stars. For comparison the dotted blue line marks the sliding window median and dashed–dotted red lines marks the 1.2 times sliding window median RUWE values.

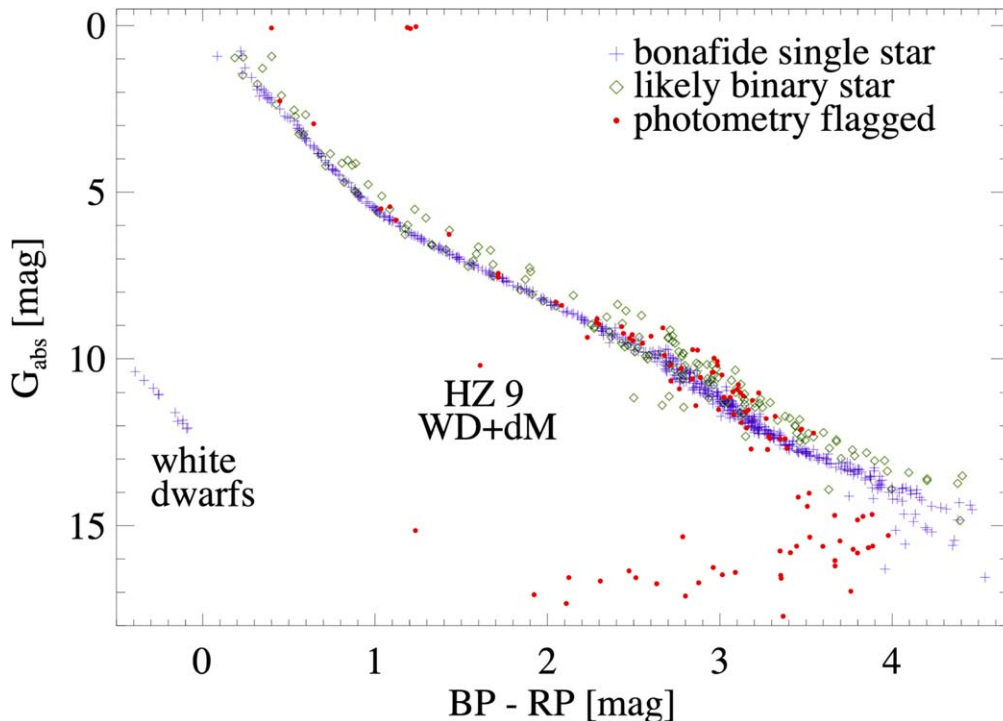


Figure 3. Color-absolute-magnitude diagram of candidate members of the Hyades open cluster based on GAIA DR3, showing the results of our classification into bona fide single main-sequence stars (and white dwarfs), likely binary and multiple systems, and stars with problematic photometry in at least one of the Gaia bands.

Hyades after the completion of the classification process. Of the sources with good photometry, we classify 601 sources as bona fide hydrogen-burning single stars, 171 sources as likely binary stars, and 11 sources as single white dwarfs with $\text{BP-RP} < 0$ mag. The single stars form a tight and well-defined sequence with

median uncertainties of $\langle \sigma_{G_{\text{abs}}} \rangle = 3.3$ mmag and $\langle \sigma_{\text{BP-RP}} \rangle = 4.1$ mmag, which presents a factor of ≈ 20 reduction of uncertainty in absolute magnitude and color compared to Kopytova et al. (2016). In addition to the single white dwarfs, in Figure 3 we also label the post-common envelope white dwarf—mid-M-dwarf

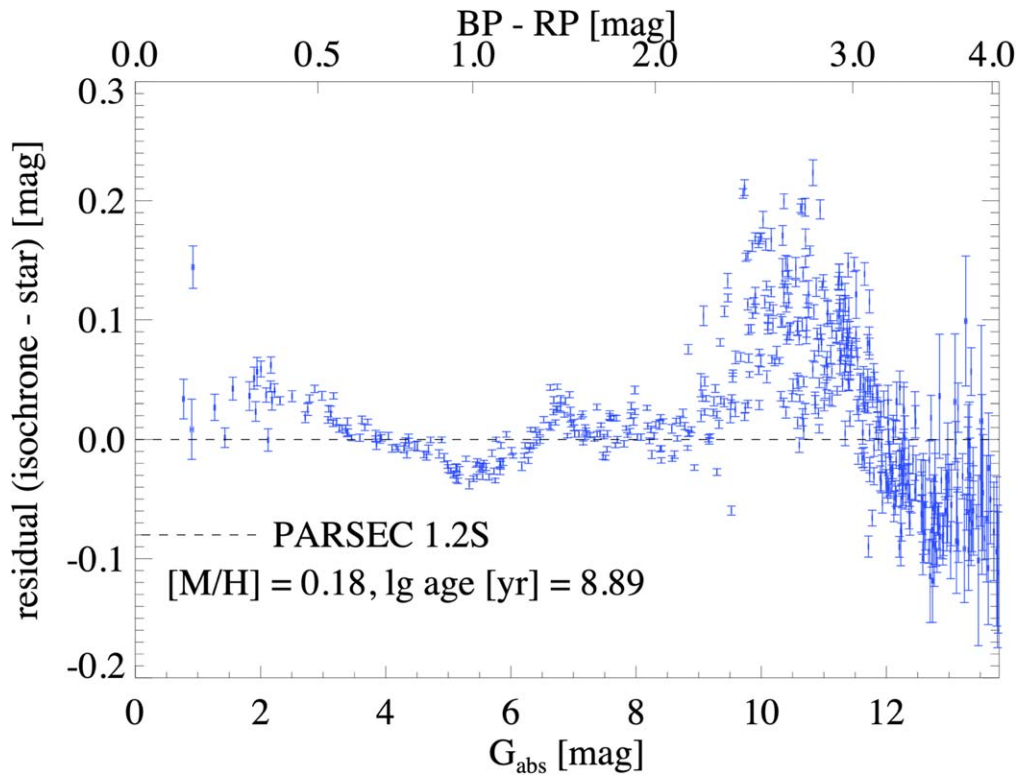


Figure 4. Minimum distance in color–magnitude space of each single star from the best-fitting isochrone, plotted against the absolute magnitude (lower abscissa) and color (upper abscissa) on the isochrone. A positive residual corresponds to stars that are brighter (redder) than predicted by the isochrone. A negative residual corresponds to stars that are fainter (bluer) than the isochrone. The uncertainties for each source in G_{abs} correspond to the Gaia uncertainties in absolute G magnitude, and the uncertainties in the residuals correspond to the quadratically added uncertainties in absolute G magnitude and BP–RP color.

binary HZ 9 (Rios-Venegas et al. 2020). This source is misclassified by our two-color rejection due to its atypical composite spectral energy distribution, resulting in BP– $G = 0.68$ mag and G –RP = 0.93 mag. Nevertheless, HZ 9 would be excluded from the single-star sample due to its binary nature.

3. Stellar Astrophysical Parameters: Fitting PARSEC Isochrones

Using the PARSEC version 1.2S CMD web interface,⁵ we obtain families of isochrones in the Gaia DR3 photometric system. The range of age and abundance values is based on literature values from isochrone fitting to stars in the Hyades open cluster as compiled by Brandner et al. (2023), i.e., log age [yr] = 8.70 to 8.95 and $[M/H] = 0.10$ – 0.25 . We assume an average visual extinction of $A_V = 3.1$ mmag (Taylor 2006). We use χ^2 minimization to identify the best-fitting nonrotating PARSEC isochrones to the 80 brightest ($G_{\text{abs}} \leq 5.5$ mag) bona fide single upper-main-sequence and main-sequence turn-off stars, which yields log age [yr] = 8.89 ± 0.01 and $[M/H] = 0.18 \pm 0.03$.

In Figure 4 we show the minimum distance in the color–magnitude space of each star to the best-fitting isochrone. Overall the residuals between the observed stellar sequence and the PARSEC isochrone are considerably smaller than is the case for the best-fitting MESA 1.2 isochrone (Brandner et al. 2023). Noticeable is the systematic deviation for stars with $10 \text{ mag} < G_{\text{abs}} < 12 \text{ mag}$. Stars in this brightness range also exhibit large scatter, which is not explained by the intrinsic photometric uncertainty of the Gaia DR3 measurements.

Figure 5 shows the single-star main sequence of the Hyades with the family of best-fitting isochrones overlaid. We use the point of minimum distance on the isochrones to determine T_{eff} , log g , log L , (present-day) mass, and the associated uncertainties for each star and present the results in Table 1.

4. Discussion

The inherently exquisite photometric and astrometric precision of Gaia DR3 reveals a very well-defined and tight single-star sequence in the Hyades. Families of PARSEC version 1.2S isochrones explain this as a stellar population with a small intrinsic spread in metallicity and age and thus provide very accurate measurements of the absolute metallicity and age of the Hyades stellar open cluster in this frame of reference (Figure 5).

The strongest systematic deviations between observations and isochrones are in the mass range 0.22 – $0.40 M_{\odot}$, where the stars are systematically brighter and/or redder than predicted by the isochrone at 0.02 – 0.2 mag and below $0.18 M_{\odot}$, where stars are fainter and/or bluer at 0.01 – 0.1 mag. This is akin to a mismatch found between dynamical mass estimates and masses derived from isochrones for M-dwarf binaries and multiple systems in the solar neighborhood, like, e.g., GJ 2060, which is a member of the 50–100 Myr old AB Dor moving group (Rodet et al. 2018), or 2MASS J10364483+1521394, which has an age of 400–600 Myr (Calissendorff et al. 2017, 2018).

For masses between 0.4 and $2 M_{\odot}$, the observed stellar sequence is in excellent agreement with the isochrones and never deviates by more than 0.03 mag in the color–brightness space. This is different from the findings by Jaehnig et al. (2019), who studied 69 presumed members of the Hyades open

⁵ <http://stev.oapd.inaf.it/cmd>

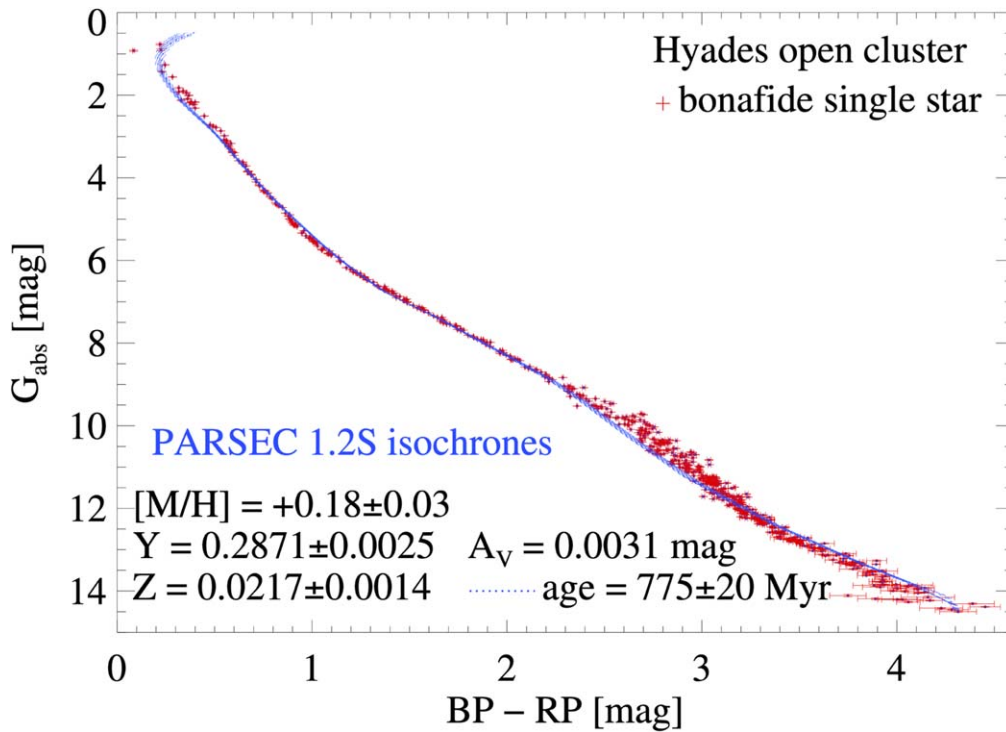


Figure 5. Color-absolute-magnitude diagram of ≈ 600 bona fide single-star candidate members of the Hyades open cluster based on Gaia DR3. Overall, the family of PARSEC isochrones for $[M/H] = +0.18 \pm 0.03$, age = 775 ± 20 Myr, and $A_V = 3.1$ mmag provides a very good fit to the observed main sequence. In the color range $2.4 \text{ mag} \leq \text{BP-RP} \leq 3.2 \text{ mag}$ (≈ 0.22 to $0.40 M_\odot$), stars are systematically brighter (respectively redder) than predicted by the isochrones.

Table 1
Astrophysical Parameters of Bona Fide Single Stars in the Hyades Open Cluster

GAIA DR3 ID	R.A. (deg)	Decl. (deg)	d (pc)	G (mag)	mass (M_\odot)	σ_{mass} (M_\odot)	$\log T_{\text{eff}}$ (K)	$\sigma_{\log T_{\text{eff}}}$ (K)	$\log L$ (L_\odot)	$\sigma_{\log L}$ (L_\odot)	$\log g$ (cm s^{-2})	$\sigma_{\log g}$ (cm s^{-2})
395696646953688448	0.653134	51.945348	59.611	10.7791	0.7431	0.0025	3.6508	0.0004	-0.7832	0.0021	4.6464	0.0008
393017579491591168	2.016317	47.275403	64.815	17.0372	0.1691	0.0036	3.4495	0.0020	-2.6195	0.0198	5.0443	0.0052
420637590762193792	2.509754	55.443035	83.610	18.4767	0.1460	0.0054	3.4278	0.0063	-2.8203	0.0554	5.0717	0.0098
385502112574538624	3.829797	43.743120	42.821	14.3729	0.3025	0.0032	3.4899	0.0008	-2.1138	0.0064	4.9403	0.0046
394413482520591744	4.297654	49.937840	68.621	16.6537	0.1960	0.0033	3.4621	0.0012	-2.4837	0.0113	5.0242	0.0048
394913657235233664	4.962093	50.735753	65.757	17.0534	0.1703	0.0032	3.4502	0.0016	-2.6123	0.0159	5.0434	0.0050

Note. Table 1 is published in its entirety in machine-readable format. The first six entries, omitting some of the columns with uncertainties on the distance estimates, and part of the Gaia DR3 photometry are shown here for reference regarding its form and content.

(This table is available in its entirety in machine-readable form.)

cluster in the mass range 0.5 to $1.0 M_\odot$. They report 15 stars with a radius inflation $\geq 10\%$ with respect to a “nominal” isochrone. Seven of these 15 stars are in the GCNS sample of likely members of the Hyades. We find that two of these (2MASS J04084015+2333257 and 2MASS J04115620+2338108) have problematic photometry in at least one of the Gaia photometric bands. According to Jaehnig et al. (2019), four of the remaining five stars are binary stars (2MASS J04175061+1828307, 2MASS J04181077+2317048, 2MASSJ04322565+1306476, and 2MASSJ 04491296+2448103). Gaia DR3 detects evidence for orbital motion (i.e., $\text{RUWE} > 1.4$) in 2MASS J04175061+1828307 and 2MASS J04491296+2448103. In Brandner et al. (2023), we flag 2MASS J04235070+0912193 as a probably binary star due to its location on the binary sequence. Jaehnig et al. (2019) assign a radius inflation of $\Delta R/R = 23.0\% \pm 6.6\%$ to this star. Observations at high angular resolution, possibly combined with radial-velocity monitoring, could help to decipher

the true nature of this star, i.e., if it is an actual single star subject to radius inflation or a close, thus far unresolved, binary star.

While the PARSEC isochrones overall provide a considerably better fit to the Hyades single-star sequence than, e.g., the MESA 1.2 isochrones, we note some caveats:

1. PARSEC version 1.2S does not consider stellar rotation. Stellar rotation should affect in particular the upper-main-sequence and main-sequence turn-off region in the Hyades, which is also the region most sensitive to the isochronal age.⁶ For the majority of the stars in our sample, the effect on the determined astrophysical parameters should be minimal. We note that stellar

⁶ Gossage et al. (2018) find that MESA models considering rotation result in lower effective temperature due gravity darkening. When fitting MESA isochrones in the TYCHO photometric system to the Hyades, they derive a lower age estimate for the models with $\frac{\Omega}{\Omega_c} = 0.3$ than for the nonrotating models.

rotation is considered in the PARSEC evolutionary tracks and isochrones starting with version 2.0. However, at the time the present research was carried out, PARSEC version 2.0 was limited to $[M/H] \leq +0.07$, which is below the canonical metal abundance estimates for the Hyades.

2. The $[He/H]$ abundance in the PARSEC models follows the solar-scaled $Y = 0.2485 + 1.78Z$ relation, while there is some evidence in the literature for a supersolar He abundance (see, e.g., the discussion in Tognelli et al. 2021). A consequence of an underestimate of the He abundance would be an underestimate of the energy production for lower-mass Hyades members, which still remember their primordial He abundance (i.e., these stars should not yet have reached perfect equilibrium on the p–p I ^3He chain of nuclear fusion; see, e.g., Baraffe & Chabrier 2018).
3. The astrometric and photometric identification of likely binary and multiple systems is most efficient for approximately equal brightness and equal mass systems, i.e., systems with mass ratios ≥ 0.5 (see, e.g., Elson et al. 1998). More extreme brightness and mass ratio binary systems should still be present in our sample.
4. Our sample is ignorant about stellar activity and variability and individual extinction for each star. Here, multiwavelength SED fitting, as might be facilitated by the next generation of space-based infrared surveys like Euclid and Roman, should provide vastly improved characterizations.

Despite these limitations, the sample should be useful for a multitude of applications like benchmarking stellar evolutionary models or the testing and verification of the calibration of large surveys such as the Gaia Astrophysical Parameters Inference System (see, e.g., Fouesneau et al. 2022). The table with astrophysical properties of ≈ 600 bona fide single stars in the Hyades could also be useful to calibrate, for example, different spectroscopic surveys with little or no internal overlap in their samples, against each other by using sources in common with our sample as a reference. The sample also provides a homogeneous characterization of the exoplanet hosts in the Hyades open cluster (see, e.g., Mann et al. 2016; Ciardi et al. 2018; Livingston et al. 2018; Mann et al. 2018; Vanderburg et al. 2018), which facilitates a differential comparison of exoplanet properties in an open cluster.

For stars in the mass range exhibiting radius anomalies, a more detailed study of rotation periods and activity levels is required. This might reveal insights into the stellar structure and could probe the region susceptible to the convective kissing instability (van Saders & Pinsonneault 2012; Baraffe & Chabrier 2018; Mansfield & Kroupa 2021, 2022).

This work has made use of data from the European Space Agency (ESA) mission Gaia (<https://www.cosmos.esa.int/gaia>), processed by the Gaia Data Processing and Analysis Consortium (DPAC, <https://www.cosmos.esa.int/web/gaia/dpac/consortium>). Funding for the DPAC has been provided

by national institutions, in particular the institutions participating in the Gaia Multilateral Agreement.

Facility: Gaia.

ORCID iDs

Wolfgang Brandner  <https://orcid.org/0000-0003-1939-6351>
 Per Calissendorff  <https://orcid.org/0000-0002-5335-0616>
 Taisiya Kopytova  <https://orcid.org/0000-0002-5723-9763>

References

- Bailer-Jones, C. A. L., Rybizki, J., Fouesneau, M., Demleitner, M., & Andrae, R. 2021, *AJ*, 161, 147
- Baraffe, I., & Chabrier, G. 2018, *A&A*, 619, A177
- Bovy, J. 2016, *ApJ*, 817, 49
- Brandner, W., Calissendorff, P., & Kopytova, T. 2023, *MNRAS*, 518, 662
- Bressan, A., Marigo, P., Girardi, L., et al. 2012, *MNRAS*, 427, 127
- Calissendorff, P., Janson, M., Kohler, R., et al. 2017, *A&A*, 604, A82
- Calissendorff, P., Janson, M., Kohler, R., et al. 2018, *A&A*, 618, C6
- Castellani, V., Degl'Innocenti, S., & Prada Moroni, P. G. 2001, *MNRAS*, 320, 66
- Chen, Y., Girardi, L., Bressan, A., et al. 2014, *MNRAS*, 444, 2525
- Choi, J., Dotter, A., Conroy, C., et al. 2016, *ApJ*, 823, 102
- Ciardi, D. R., Crossfield, I. J. M., Feinstein, A. D., et al. 2018, *AJ*, 155, 10
- Dotter, A. 2016, *ApJS*, 222, 8
- Elson, R. A. W., Sigurdsson, S., Davies, M., Hurley, J., & Gilmore, G. 1998, *MNRAS*, 300, 857
- Fouesneau, M., Frémat, Y., Andrae, R., et al. 2022, arXiv:2206.05992
- GAIA-Collaboration 2020, Gaia eDR3 source catalogue “light”, <https://dc.zah.uni-heidelberg.de/tableinfo/gaia.edr3lite>
- Gaia Collaboration, Smart, R. L., Sarro, L. M., et al. 2021, *A&A*, 649, A6
- Gentile Fusillo, N. P., Tremblay, P.-E., Cukanovaite, E., et al. 2021, *MNRAS*, 508, 3877
- Girardi, L., Bertelli, G., Bressan, A., et al. 2002, *A&A*, 391, 195
- Golovin, A., Reffert, S., Just, A., et al. 2023, *A&A*, 670, A19
- Gossage, S., Conroy, C., Dotter, A., et al. 2018, *ApJ*, 863, 67
- Jaehnig, K., Somers, G., & Stassun, K. G. 2019, *ApJ*, 879, 39
- Jeffery, E. J., Taylor, B. J., & Joner, M. D. 2022, *ApJ*, 936, 153
- Jeffries, R. D. 2017, *Mem. Soc. Astron. Italiana*, 88, 637
- Kopytova, T. G., Brandner, W., Tognelli, E., et al. 2016, *A&A*, 585, A7
- Krumholz, M. R., & McKee, C. F. 2020, *MNRAS*, 494, 624
- Kudryavtseva, N., Brandner, W., Gennaro, M., et al. 2012, *ApJL*, 750, L44
- Lindgren, L., Klioner, S. A., Hernandez, J., et al. 2021, *A&A*, 649, A2
- Livingston, J. H., Dai, F., Hirano, T., et al. 2018, *AJ*, 155, 115
- Magrini, L., Randich, S., Kordopatis, G., et al. 2017, *A&A*, 603, A2
- Mann, A. W., Gaidos, E., Mace, G. N., et al. 2016, *ApJ*, 818, 46
- Mann, A. W., Vanderburg, A., Rizzuto, A. C., et al. 2018, *AJ*, 155, 4
- Mansfield, S., & Kroupa, P. 2021, *A&A*, 650, A184
- Mansfield, S., & Kroupa, P. 2022, *A&A*, 661, C1
- Marigo, P., Girardi, L., Bressan, A., et al. 2008, *A&A*, 482, 883
- Parmentier, G., Pfalzner, S., & Grebel, E. K. 2014, *ApJ*, 791, 132
- Riello, M., De Angeli, F., Evans, D. W., et al. 2021, *A&A*, 649, A3
- Rios-Venegas, C., Contreras-Quijada, A., Vogt, N., et al. 2020, *MNRAS*, 493, 1197
- Rodet, L., Bonnefoy, M., Durkan, S., et al. 2018, *A&A*, 618, A23
- Taylor, B. J. 2006, *AJ*, 132, 2453
- Tognelli, E., Dell Omodarme, M., Valle, G., Prada Moroni, P. G., & Degl'Innocenti, S. 2021, *MNRAS*, 501, 383
- van Saders, J. L., & Pinsonneault, M. H. 2012, *ApJ*, 751, 98
- Vanderburg, A., Mann, A. W., Rizzuto, A., et al. 2018, *AJ*, 156, 46
- Williams, B. A., Walker, D. L., Longmore, S. N., et al. 2022, *MNRAS*, 514, 578